Available online at www.sciencedirect.com

ScienceDirect

ARTICLE

In-situ Synthesis and Properties of Porous Cobalt Sulfide Nanoneedle Bundles Arrays on Nickel Foam as Electrodes for Supercapacitors

Sun Peng,   Liang Jicai,   Chen Guangyi,   Li Yuhui,   Zhou Kaiyuan,   Liu Jiaang,

Zhang Wenzhuo,   Niu Fu,   Zhang Wanxi

State Key Laboratory of Structural Analysis for Industrial Equipment, Dalian University of Technology, Dalian 116024, China

Abstract: Freestanding porous Co_9S_8 nanoneedle bundles arrays on Ni foam were in-situ synthesized by a facile ion exchange reaction and were directly used as the electrode for supercapacitors. The structure and morphology were characterized by X-ray diffraction (XRD), scanning electron microscope (SEM), and transmission electron microscope (TEM). Cyclic voltammetry (CV), chronopotentiometry (CP) and electrochemical impedance spectroscopy (EIS) were adopted to evaluate the electrochemical property of the porous Co_9S_8 nanoneedle bundles arrays electrode in 3 mol/L KOH solution. The results show that the specific capacitance of the porous Co_9S_8 nanoneedle bundles arrays is 1400 $F \cdot g^{-1}$ at a current density of 4 $A \cdot g^{-1}$ and the arrays exhibit good cycling stability. The excellent electrochemical performance can be ascribed to the porous nanostructure of Co_9S_8 nanoneedle bundles arrays and the 3D conductive nickel foam, which can increase the contact areas between electrode and electrolyte and improve the conductivity of the whole electrode.

Key words: supercapacitors; electrode materials; Co_9S_8; electrochemical performance

Coupled with the critical climate change and energy crises, exploiting environmentally friendly, renewable, low-cost energy storage and conversion systems become very urgent. Supercapacitors and batteries (Li-ion batteries, fuel cells, etc.) are considered as the two most practical and effective devices for electrochemical energy conversion and storage[1-4]. Supercapacitor (SC, also called electrochemical capacitor) has been paid much attention to during the past decade for its advantages such as high rapid charging and discharging rate, high power density and long cycle life[5,6]. Supercapacitor can be classified into pseudocapacitor and electric double layer capacitor (EDLC) based on the mechanism of charge storage[7]. Generally, pseudocapacitors arising from the rapid reversible faradic process of redox-active materials can provide much higher specific capacitances than EDLCs [8, 9]. Although many attempts have been dedicated to explore efficient and

inexpensive redox-active materials including transition metal hydroxides[10], oxides[11], sulfides[12], and conductive polymers[13], designing and developing facile methods to produce electrode materials with planned chemical component, unique morphologies and controlled microstructures are still highly desired.

Recently, nanostructured transition metal sulfides have been considered one of the most popular non-noble metals for pseudocapacitor electrode due to their excellent electrochemical properties and high conductivity[14]. Among them, cobalt sulfides with different stoichiometric components, including Co_4S_3, Co_9S_8, CoS, Co_3S_4, Co_2S_3, and CoS_2, make them with different properties meet the requirements for various application[15]. Up to now, various morphologies of cobalt sulfides-based materials including three-dimensional flower-like hierarchical structure [16], nanotubes[17], nanosheet-like films[18], nanoparticles

decorated graphene composite[19] have been prepared and applied in supercapacitors. However, it is still a challenge to optimize the composition and morphology of cobalt sulfides-based electroactive materials, which can dramatically improve their performance to achieve large specific capacitance and long-term stability for supercapacitors.

In this paper, the porous Co_9S_8 nanoneedle bundles arrays on Ni foam have been synthesized by a simple two-step hydrothermal route and directly acted as electrodes for supercapacitors. This binder-free and porous structure can enhance electron and ion transportation, and improve the electrochemical performance. The porous Co_9S_8 nanoneedle bundles arrays exhibited high specific capacitance (1400 $F \cdot g^{-1}$ at a current density of 4 $A \cdot g^{-1}$) and excellent long cycle stability, offering great potential application in supercapacitors.

1   Experimental

1.1   Materials

Cobalt nitrate hexahydrate, urea, ammonium fluoride, sodium sulfide, potassium hydroxide and hydrochloric acid were all analytical grade and used without any further purification. Deionized water was used throughout. Battery-grade Ni foam was purchased from ChangSha Lyrun Material. Co. Ltd (thickness: 1 mm; areal density: 320 g/m^2; PPI (pore/inch): 110; pore size: 0.2~0.6 mm).

1.2   Synthesis of $Co(CO_3)_{0.5}(OH) \cdot 0.11H_2O$ precursor

Typically, 5 mmol of $Co(NO_3)_2 \cdot 6H_2O$, 25 mmol of $CO(NH_2)_2$ and 10 mmol of NH_4F were added into 40 mL of deionized water. Then the homogeneous solution was poured into Teflon-lined stainless steel autoclave. After that, a piece of Ni foam (2 cm × 2 cm) was treated with 6 mol/L HCl, washed by deionized water, and then put into the above solution. The top side of Ni foam was uniformly coated with a polytetrafluoroethylene tape to avoid solution contamination. The autoclave liner was heated at 120 °C for 9 h, and then cooled to ambient temperature naturally. The reacted Ni foam was cleaned in deionized water under ultrasonator for 10 min, and then dried in vacuum at 60 °C for 5 h. The reactions involved in this step can be explained as follows:

$$Co^{2+}+xF^- \rightarrow [CoF]^{(x-2)-} \qquad (1)$$

$$H_2NCONH_2+2H_2O \rightarrow 2NH_4^++CO_3^{2-} \qquad (2)$$

$$[CoF_x]^{(x-2)-}+0.5CO_3^{2-}+OH^-+0.11H_2O \rightarrow$$
$$Co(CO_3)_{0.5}(OH) \cdot 0.11H_2O+xF^- \qquad (3)$$
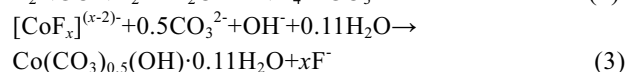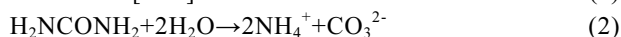
1.3 Synthesis of porous Co_9S_8 nanoneedle bundles arrays

Typically, 1 mmol Na_2S was dissolved in 40 mL deionized water and transferred into a 50 mL Teflon-line stainless steel autoclave. Then the Ni foam coated with precursor was immersed into the autoclave. The autoclave was heated to 120 °C and kept at this temperature for 5 h and then was allowed to cool to room temperature naturally.

The reaction involved in this step can be illustrated as follow:

$$Co(CO_3)_{0.5}(OH) \cdot 0.11H_2O+S^{2-} \rightarrow Co_9S_8+CO_3^{2-}+H_2O \qquad (4)$$
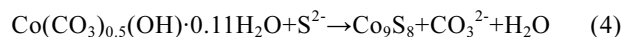
The resulting Ni foam was taken out, washed several times with the water and ethanol, and then dried at 60 °C for 4 h. The load mass of Co_9S_8 nanoneedle bundles is about 2.45 $mg \cdot cm^{-2}$.

1.4   Characterization of materials

The XRD patterns of the samples were gained by a Rigaku/Max-3A X-ray diffractometer with CuKα radiation. FE-SEM photos and EDS graphs were performed on a Supra 55 Sapphire apparatus with a system for energy dispersive X-ray analysis. TEM were performed under an accelerating voltage 200 kV on a JEOL-2010 microscope and the TEM images were gained with the selected area electron diffraction (SAED) patterns. The N_2 adsorption-desorption isotherm was determined using the Brunauer-Emmett-Teller (BET) equation by a surface area analyser SSA-4200 (Builder).

1.5   Electrochemical measurements

All electrochemical tests were recorded by employing an electrochemical workstation (CHI 660E, Shanghai, Chenhua). The supercapacitor performance measurements were performed on a three-electrode system at room temperature. The Ni foam (1 cm ×1 cm) loaded with Co_9S_8 nanoneedle bundles arrays, platinum plate, saturated calomel electrode (SCE) and 3 mol/L KOH solution were applied as the working electrode, counter electrode, reference electrode, and electrolyte, respectively. The specific capacitance (C, $F \cdot g^{-1}$) can be calculated by the following equation:

$$C=\frac{I}{M}\frac{\Delta t}{\Delta V} \qquad (5)$$

Where I(A), Δt(s), M(g) and ΔV(V) represent the discharge current, discharge time, the mass of active materials and potential window, respectively.

The energy density (E, $W \cdot h \cdot kg^{-1}$) and power density (P, $W \cdot kg^{-1}$) of the electrode materials were evaluated by the following equations:

$$E=\frac{1}{2}CV^2 \qquad (6)$$

$$P=E/\Delta t \qquad (7)$$

2   Results and Discussion

2.1   Structural characterization

The composition and morphology of the precursor and the as-obtained porous Co_9S_8 nanoneedle bundles arrays were characterized by XRD, SEM and TEM. For the sake of decreasing the impact of the nickel foam substrate on the XRD signals, both precursor and the porous Co_9S_8 nanoneedle bundles arrays powders were scratched from nickel foam substrate. Fig.1a gives the XRD pattern of the precursor, and all of the diffraction peaks can be perfectly suited to
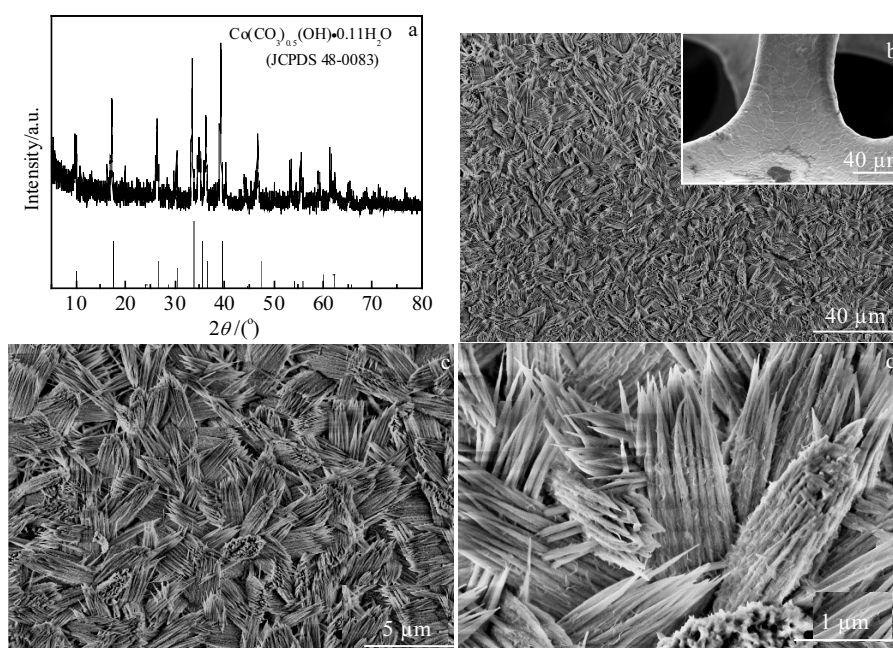
Fig.1   XRD pattern (a); SEM images (b~d) of the precursor on nickel foam (the inset in Fig.1b shows the pristine Ni foam before growth)

$Co(CO_3)_{0.5}(OH)\cdot0.11H_2O$ (JCPDS 48-0083). Fig.1b illustrates a typical low-magnification SEM image of the precursor loaded on Ni foam substrate. In comparison with the pristine Ni foam (inset in Fig.1b) with a smooth surface, it can be found that a mass of precursor are covered on the Ni foam. From the high-magnification SEM image (Fig.1d), we can see that each nanobundle is composed of tens of nanoneedles with smooth surface and the average diameter about 90 nm.

Fig. 2a gives the XRD pattern of the final sample synthesized by the hydrothermal sulfuration process. The diffraction peaks can be completely indexed to face-centered cubic Co_9S_8 (JCPDS 65-1765). The crystal structure of Co_9S_8 is shown in Fig.2b, in which 1/9 of Co atoms are coordinated to the S octahedral and 8/9 of the Co atoms are paired with the S tetrahedron to form a closed-packed cubic structure[14]. Fig.2c gives an overall morphology of the Co_9S_8 sample, whose morphology and size are very close to those of the precursor ($Co(CO_3)_{0.5}$ $(OH)\cdot0.11H_2O$). Nevertheless, high-magnification SEM image (Fig.2d) shows that the nanoneedles become rough, porous and composed of many irregular nanoparticles after hydrothermal sulfuration process. The EDS analysis of the porous Co_9S_8 nanoneedle bundles verifies that the element component is Co and S (nickel and a very low oxygen signal come from the Ni substrates and moisture and oxygen on the high-surface-area sample) (Fig.2e). Taking the above result of the XRD, it is justified that porous Co_9S_8 nanoneedle bundles have been successfully prepared via the second hydrothermal sulfuration process. The TEM image (Fig.2f) further demonstrates typical porous structure of the Co_9S_8 nanoneedle bundles. The

SAED pattern of the Co_9S_8 sample (inset in Fig.2f) consists of several bright diffraction rings, indicating the polycrystalline nature of the porous Co_9S_8 nanoneedle bundles. The formation of Co_9S_8 from precursor ($Co(CO_3)_{0.5}$ $(OH)\cdot0.11H_2O$) is an anion exchange process. The formation of the porous structure of Co_9S_8 can be explained by the ion diffusion effect and Kirkendall effect[20]. During the sulfuration process, S^{2-} ions firstly reacted with the surface metal ions of $Co(CO_3)_{0.5}(OH)\cdot0.11H_2O$ nanoneedles to form a thin Co_9S_8 layer. The formed barrier layer then presented the S^{2-} ions from further diffusing and reacting with the core Co^{2+} ions. So the following reaction progresses by the diffusion of the Co^{2+} from core to surface would be the dominant process and this unequal diffusion process could produce voids close to the interface to form porous structure of Co_9S_8 nanoneedle bundles arrays. The porous microstructure of Co_9S_8 nanoneedle bundles was further studied by the BET analysis. The N_2 adsorption and desorption isotherms and the corresponding pore size distribution are provided in Fig.3, giving the specific surface area and total pore volume are 147 $m^2\cdot g^{-1}$ and 0.48 $m^3\cdot g^{-1}$, respectively. The porous microstructure can enhance the contact between electrode and electrolyte and bring more electroactive sites during the charge-discharge process. Therefore, the obtained porous Co_9S_8 nanoneedle bundles arrays can be a promising candidate for supercapacitors.

2.2   Electrochemical performance analysis

The supercapacitor characters of the porous Co_9S_8 nanoneedle bundles arrays on nickel foam were studied by a three-electrode configuration in 3 mol/L KOH electrolyte.
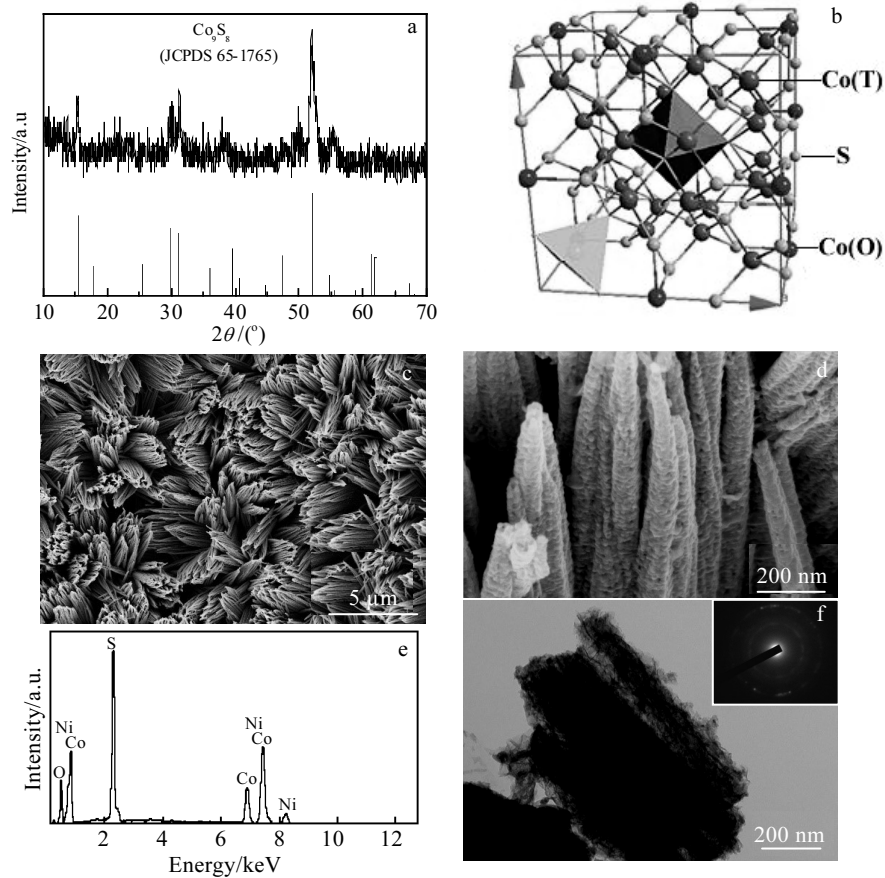
Fig.2   XRD pattern (a); crystal structure (b); SEM images (c, d); EDS spectrum (e); TEM image and SAED pattern (f) of the as-obtained
        porous Co_9S_8 nanoneedle bundles arrays synthesized at 120 °C for 5 h
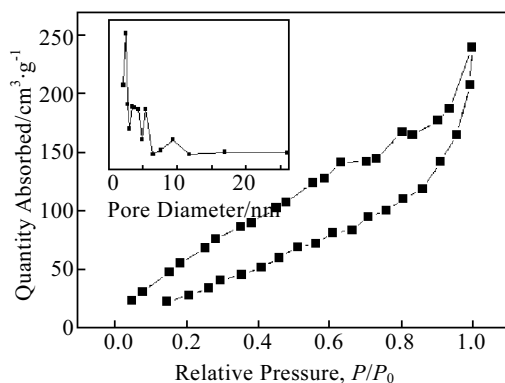
Fig.3 N_2 adsorption-desorption isotherms and the corresponding
        pore size distribution of Co_9S_8 nanoneedle bundles arrays

Fig.4a displays the curves of cyclic voltammetry (CV) at different scan rates in a potential window of 0~0.4 V vs. the SCE. A pair of redox peaks can be seen in all curves, indicating that the capacitances of the Co_9S_8 nanoneedle bundles arrays on nickel foam are primarily related to the pseudocapacitive mechanism. Furthermore, with the scan rate increasing, the intensities of the redox current peaks also increase and the peaks position gradually shift to higher potential. The redox peaks are still obvious at the high scan rate of 50 mV·s^{-1}, indicating that the Co_9S_8 nanoneedle bundles arrays on nickel foam served as electrode are very stable. The reversible redox reaction could be expressed as the following equation[21]:

$$Co_9S_8 + OH^- \leftrightarrow Co_9S_8OH + e^- \tag{8}$$

The GCD curves at different current densities were performed in the potential range of 0~0.4 V (Fig.4b). From it, we can find that all the curves have a symmetric shape. The discharge time decreases with the current density increasing and all the specific capacitances corresponding to different current densities can be calculated using Eq.(6). The specific capacitances of porous Co_9S_8 nanoneedle bundles arrays are 1400, 1241, 1120 and 991 F·g^{-1} at current densities of 4, 8, 16 and 24 A·g^{-1}, repectively (Fig.4c). From the Ragone plot of the porous Co_9S_8 nanoneedle bundles arrays (Fig.4d), we can find that the energy density decreases from 29.6 to 20.9 W·h·kg^{-1} and at the same time the power density increases from 785 to 4681 W·kg^{-1} with the current density increasing from 4 to 24 A·g^{-1}.
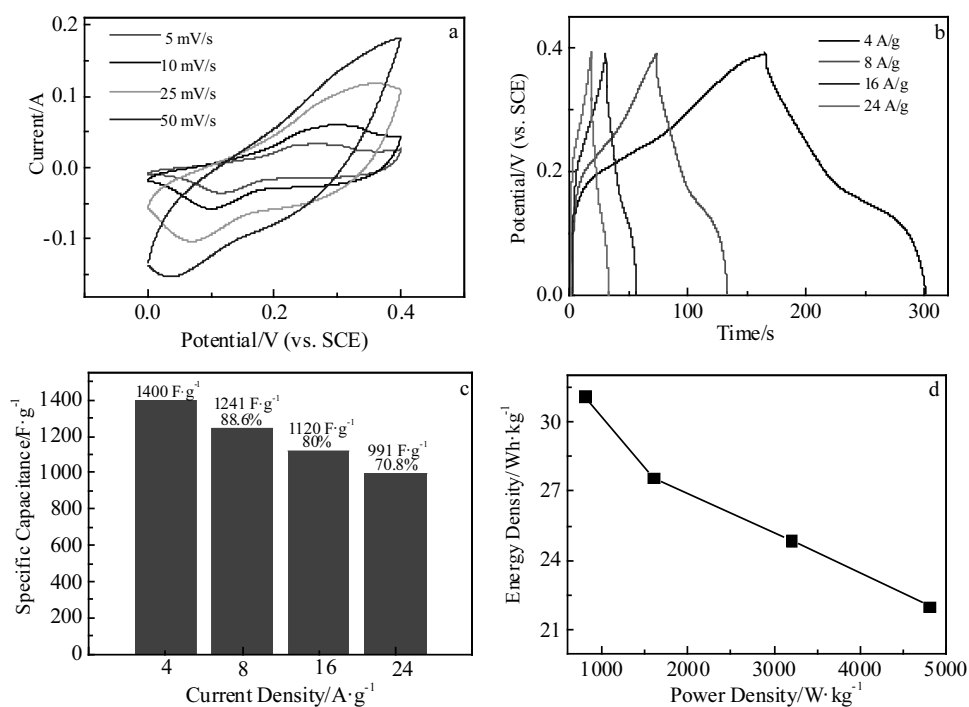
Fig. 4   CV curves at different scan rates (a); GCD curves at different current densities (b); specific capacitances calculated from galvanostatic charge-discharge curves (c); Ragone plot showing energy density vs. power density (d) of the porous Co_9S_8 nanoneedle bundles arrays

The cycling stabilities of porous Co_9S_8 nanoneedle bundles arrays on Ni foam were evaluated using a long-term galvanostatic charge/discharge process at 16 $A \cdot g^{-1}$ (Fig.5a). Notably, the porous Co_9S_8 nanoneedle bundles arrays electrode is very stable and the specific capacitance slightly increases from 1120 $F \cdot g^{-1}$ to 1160 $F \cdot g^{-1}$ after 1000 cycles, which may be related to the full activation of the porous active electrode materials during the cycles[22,23], and kept basically unchanged in the subsequent 1000 cycles. Such an outstanding faradaic pseudocapacitance characters of the Co_9S_8 nanoneedle

bundles arrays may be due to the good conductivity and rather low resistance that is evaluated via electrochemical impedance spectrum (EIS). Fig.5b exhibits the Nyquist plots of the porous Co_9S_8 nanoneedle bundles arrays electrode before and after 2000 charge/discharge cycles tested at an open circuit potential in the frequency from 0.01 to 10^5 Hz. The impedance spectra were fitted by the electrical equivalent circuit (inset in Fig.5b), in which R_s, R_{ct}, C_{dl}, C_F, and are the electrolyte resistance, the faradaic interfacial charge transfer resistance, the constant phase element accounting for a double-layer capacitance, the faradaic
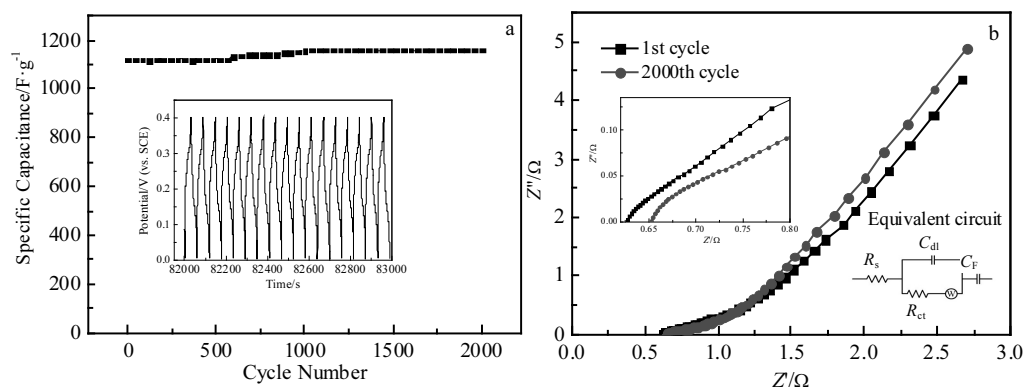
Fig. 5   Cycling behavior of the porous Co_9S_8 nanoneedle bundles arrays at 16 $A \cdot g^{-1}$ for 2000 cycles (a); EIS spectra before and after cycle tests (b)

pseudocapacitance, and the Warburg impedance, respectively[24]. Before and after 2000 cycles, the R_s and R_{ct} values are all very small and the Nyquist plots almost overlap together. This result further confirm the fine cycling stability of the porous Co_9S_8 nanoneedle bundles arrays electrode.

3 Conclusions

1) The freestanding porous Co_9S_8 nanoneedle bundles arrays on Ni foam has been synthesized based on the anion-exchange reaction.

2) Owing to the porous nanostructure of Co_9S_8 nanoneedle bundles and the three-dimensional structure of Ni foam, the Co_9S_8 nanoneedle bundles arrays exhibit an outstanding electrochemical performance (1400 $F·g^{-1}$ at 4 $A·g^{-1}$ and excellent cycling stability), indicating a promising electrode material for high-performance supercapacitors.

References

1 Lu Q, Chen J G, Xiao J Q. *Angewandte Chemie International Edition*[J], 2013, 52: 1882

2 Zhang L L, Zhou R, Zhao X S. *Journal of Materials Chemistry* [J], 2010, 20: 5983

3 Laurence C, Rosa P M. *Journal of the American Chemical Society*[J], 2015, 137: 3140

4 Elmer T, Worall M W, Wu S *et al. Renewable and Sustainable Energy Reviews*[J], 2015, 42: 913

5 Yan J, Wang Q, Wei T *et al. Advanced Energy Materials*[J], 2014(4): 1300816

6 Choi H, Yoon H. *Nanomaterials*[J], 2015, 5: 906

7 Wang G, Zhang L, Zhang J. *Chemical Society Reviews*[J], 2012, 41: 797

8 Zou R, Xu K, Wang T *et al. Journal of Materials Chemistry A*[J], 2013(1): 8560

9 Guo D, Lai L, Cao A *et al. RSC Advances*[J], 2015(5): 55 856

10 Tan P, Xiao T, Tan X Y *et al. Journal of Alloys and Compounds*[J], 2016, 656: 714

11 Qiao Y Q, Sun Q J, Xi J Y *et al. Journal of Alloys and Compounds*[J], 2016, 660: 416

12 Zhou K Y, Liang J C, Liu J A *et al. RSC Advances*[J], 2016, 6: 15832

13 Dubal D P, Patil S V, Gund G S *et al. Journal of Alloys and Compounds*[J], 2013, 552: 240

14 Rui X, Tan H, Yan Q. *Nanoscale*[J], 2014(6): 9889

15 Rao C N R, Pisharody K P R. *Progress in Solid State Chemistry* [J], 1976, 10: 207

16 Luo F L, Li J, Yuan H Y *et al. Electochimica Acta*[J], 2014, 123: 183

17 Pu J, Wang Z, Wu K *et al. Physical Chemistry Chemical Physics*[J], 2014, 16: 785

18 Lin J Y, Chou S W. *RSC Advances*[J], 2013, 3: 2043

19 Qu B H, Chen Y J, Zhang M *et al. Nanoscale*[J], 2012(4): 7810

20 Gong C, Huang M L, Zhou P *et al. Applied Surface Science*[J], 2016, 362: 469

21 Yu J, Wan H, Jiang J *et al. Journal of the Electrochemical Society*[J], 2014, 161: A996

22 Yuan C, Zhang X, Su L *et al. Journal of Materials Chemistry*[J], 2009, 19: 5772

23 Zhu Y, Liu T, Ma W *et al. Chemical Letters*[J], 2015, 44: 1321

24 Wei T Y, Chen C H, Chang K H *et al. Chemistry of Materials*[J], 2009, 21: 3228

硫化钴多孔疏松纳米针束阵列超级电容器电极材料在泡沫镍基底上的原位合成及电化学性能研究

孙 朋，梁继才，陈广义，李煜辉，周开塬，刘加昂，张文卓，牛 福，张万喜

(大连理工大学 工业装备结构分析国家重点实验室，辽宁 大连 116024)

摘 要：在导电泡沫镍基底上通过一种简便的离子交换反应原位合成出了硫化钴多孔疏松纳米针束阵列并直接用作超级电容器的电极。采用 X 射线衍射（XRD）、扫描电子显微镜（SEM）、透射电子显微镜（TEM）等手段对其结构和形貌进行了详细的表征。同时运用循环伏安（CV）、计时电位分析（CP）、电化学阻抗谱（EIS）等方法对其在 3 mol/L KOH 电解液中的电化学性能进行了分析，结果表明这种在泡沫镍基底上原位生长出的 Co_9S_8 多孔疏松纳米针捆束阵列在 4 $A·g^{-1}$ 的电流密度下具有高达 1400 $F·g^{-1}$ 的比电容和优异的循环稳定性能。这种电极材料之所以具有如此优秀的电化学性能，主要归因于 Co_9S_8 纳米针捆束阵列的多孔疏松结构与 3D 泡沫镍基底之间的协同效应可以有效的增加电极材料与电解液之间的接触面积和提高整个电极的导电性。

关键词：超级电容器；电极材料；Co_9S_8；电化学性能

作者简介：孙 朋，男，1985 年生，博士生，大连理工大学汽车工程学院，辽宁 大连 116024，电话：0411-84706475，E-mail: s11322002@mail.dlut.edu.cn